Nonlinear propagation of an optical speckle field

Stanislav Derevyanko*
Nonlinearity and Complexity Research Group, Aston University, Aston Triangle, Birmingham B4 7ET, United Kingdom

Eran Small
Department of Physics of Complex Systems, Weizmann Institute of Science, Rehovot 76100, Israel
(Received 27 February 2012; published 14 May 2012)

We provide a theoretical explanation of the results on the intensity distributions and correlation functions obtained from a random-beam speckle field in nonlinear bulk waveguides reported in the recent publication by Bromberg *et al*. [Nat. Photonics **4**, 721 (2010)]. We study both the focusing and defocusing cases and in the limit of small speckle size (short-correlated disordered beam) provide analytical asymptotes for the intensity probability distributions at the output facet. Additionally we provide a simple relation between the speckle sizes at the input and output of a focusing nonlinear waveguide. The results are of practical significance for nonlinear Hanbury Brown and Twiss interferometry in both optical waveguides and Bose-Einstein condensates.

DOI: 10.1103/PhysRevA.85.053816 PACS number(s): 42.65.Tg, 42.30.Ms, 05.10.Gg

I. INTRODUCTION

Extreme events play an important part in many areas of physics. In turbulence they determine the non-Gaussian statistics of the tails of the probability distribution functions for the properties of random flow [1], and in the linear theory of random-wave localization the momenta non-self-averaging quantities, such as, e.g., wave transmissivity, are determined by rare nontypical realizations rather than the typical (localized) ones [2,3].

In the context of nonlinear optics the study of extreme events has recently drawn attention in the context of *optical rogue waves* [4]—emerging dynamical objects of very high amplitude and short lifetime. Closely related topics are extreme statistics in Raman amplification [5] and *supercontinuum generation* [6]. The appearance of the rogue waves in optical fibers is not necessarily a nonlinear effect and can be observed in the linear regime as well [7]. Finally the statistics of rare events (extreme outages) also determines the probability of errors in fiber-optical communications with distributed-amplifier spontaneous emission [8].

Most of the applications above pertain to the field of nonlinear fiber optics. Here we study the emergence of high-power optical pulses in the context of nonlinear Hanbury Brown and Twiss (HBT) interferometry. The goal of this paper is to explain theoretically recent experimental results reported in Ref. [9] on the nonexponential tails of the probability distributions of the intensity of disordered optical fields propagating in nonlinear bulk waveguides. The linear HBT method was first proposed in the 1950s in astronomy as a means of measuring the size of a distance light source (e.g., a star) by measuring the *intensity correlation radius* of the received light [10]. The latter is the the typical size of an optical *speckle* (i.e., bright area) observed when multiple waves emitted from a thermal source interfere constructively [11]. The problem allows classical treatment, and when the propagation is linear one can infer that at a distance Z from a source of diameter L the size of the speckle S is given by the simple relation $S = Z\lambda/L$, where λ is the wavelength of emitted light [9].

Reference [9] was the first publication to our knowledge where HBT interferometry in *nonlinear light* propagation and the resulting speckle distribution were studied in bulk AlGaAs waveguides. The system is effectively described by the nonlinear Schrödinger equation (NLSE), which paves the way to application of nonlinear HBT interferometry not only in the field of optics but in weakly interacting Bose-Einstein condensates as well [12]. Two principal findings of Ref. [9] were that the tail of the intensity distribution $P(I)$ of the speckled field is nonexponential (unlike in linear diffraction [11]) and that the intensity correlation radius (speckle size) depends on the magnitude of the focusing nonlinearity. The first observation signifies the fact that the statistics of the optical field after nonlinear propagation is no longer Gaussian (or, equivalently, the amplitude of the field no longer follows the Rayleigh distribution). This effect is also known to occur in linear systems when a linear wave propagates through a disordered medium [13]. Here however we deal with a different type of setup where not only is nonlinearity present but also the disorder is only in the initial conditions (incident beam) and not in the medium itself. For the focusing nonlinearity in an important two-dimensional (2D) configuration of the system (commonly known as $1+1$ geometry), this phenomenon was correctly attributed by the authors of Ref. [9] to generation of *bright spatial soliton* beamlets [14] that now play the role of observed speckles. The tails of the intensity distribution are determined by extremely rare events when an extremely high-power (and narrow) soliton is created from a random beam of finite waist and intensity. Note that the propagation of incoherent fields in nonlinear optics has been studied previously in various contexts (see, e.g., Refs. [15,16]), but the specific problem of intensity tails and the correlation functions of the nonlinear HBT interferometer had not been properly studied (either experimentally or theoretically) before the publication of [9].

Our paper seeks to explain theoretically the profile and shape of the tails of the intensity probability density functions (PDFs) in the $1+1$ geometry using the inverse scattering technique (IST) for the NLSE [17]. The paper is organized as

*s.derevyanko@aston.ac.uk

 ©2012 American Physical Society

follows: In Sec. II we introduce the NLSE model and the model for disorder. Then in Sec. III we first construct a semiempirical theory of a HBT interferometer in the high-power regime where the field is dominated by its soliton component. In Sec. IV this theory is corroborated by the results obtained analytically from the IST in the limit of a short-correlated source field. Section V is dedicated to theoretical results in the case of a defocusing nonlinearity where no bright solitons are observed, and we summarize our findings in the Conclusion. In all cases we perform full numerical simulations using parameters close to those used in the experimental setup of Ref. [9] to confirm our analytical predictions.

II. THE MODEL

The dynamics of beam propagation along the direction of the z axis in the presence of diffraction and nonlinearity is given by the nonlinear Schrödinger equation [14]:

$$\frac{\partial E}{\partial z} = \frac{i}{2\beta_0}\frac{\partial^2 E}{\partial x^2} + i\frac{n_2}{n_0}\beta_0|E|^2E, \tag{1}$$

where E is the electrical field, x is the spatial transverse coordinate, $\beta_0 = (2\pi/\lambda)n_0$ is the propagation constant, n_0 is the linear refractive index, and n_2 is the nonlinear coefficient of the medium. Here we will consider both the attractive ($n_2 > 0$) and repulsive ($n_2 < 0$) cases. We will also be using dimensionless soliton units $\xi = x/L$, where L is some characteristic width, $\tau = z/L_d$ where $L_d = L^2\beta_0$ is the diffraction length (Rayleigh range), and u is the dimensionless field $E/\sqrt{\tilde{I}}$ with $\tilde{I} = (|n_2|\beta_0 L_d/n_0)^{-1}$. Then in the new dimensionless units we have

$$\frac{\partial u}{\partial \tau} = \frac{i}{2}\frac{\partial^2 u}{\partial \xi^2} + \frac{n_2}{|n_2|}i|u|^2u. \tag{2}$$

When choosing the model for the randomly disordered input we opt for a form which mimics as closely as possible the experimental setup and simulation data from Ref. [9]. The physical input is defined by two parameters: the initial speckle size S_0 and the aperture L (we also pick the latter as the normalization width for the soliton units above). In our numerical simulations the spatial resolution δx is determined according to S_0 to ensure sufficient sampling and the width of the computational domain L' is set large enough to prevent folding during propagation. The input disordered field is modeled in Fourier space by N random low-frequency modes, where $N = L'/S_0$. As for the complex amplitudes of these random modes, a_n, we assume that these form a set of of independent identical random variables each having a uniformly distributed phase and an amplitude sampled from a distribution with the average intensity a^2. This pattern is then filtered by the finite aperture L to manifest the disordered field at the input facet of the nonlinear waveguide. As the number of modes is large the central limit theorem applies so that the field above, $E_0(x)$, can be considered Gaussian with zero mean and the correlation function

$$\langle E_0(x)E_0^*(x')\rangle = a^2\frac{\sin[\pi(x-x')N/L']}{\sin[\pi(x-x')/L']}. \tag{3}$$

The field is of course nonzero only in the aperture window $[-L/2, L/2]$ so the formula above applies only to this region. The averaged initial intensity is then $I_0 = \langle|E_0(x)|^2\rangle = a^2N$. Also, when S_0 is the smallest length scale in the problem, we will be using the δ-correlated approximation in which the right-hand side (RHS) of Eq. (3) is substituted with $2\tilde{D}\delta(x-x')$ where $\tilde{D} = L'a^2/2 = S_0I_0/2$. This makes further analytical treatment possible in some cases, and we will often use it in the paper.

As for the intensity distribution $P(I)$, since the initial field is Gaussian, the statistics of the propagated field in the linear case ($n_2 = 0$) will remain Gaussian. As the intensity is the modulus squared of the complex Gaussian variate, its normalized value $I/\langle I\rangle$ has an exponential distribution, a fact which is well known in the linear theory of speckle spectra [11]. Our main task in the subsequent sections will be to determine the modified shapes of the intensity distribution $P(I)$ in the presence of nonlinearity. Of particular interest is the high-intensity tail of this distribution, determined by rare fluctuations leading to field bursts.

III. THE PHENOMENOLOGICAL APPROACH

Let us consider the case of the focusing ($n_2 > 0$) NLSE. Then it is known that, given enough initial power, an arbitrary initial condition $E_0(x)$ evolves into a combination of hyperbolic secant constituents (each corresponding to an individual bright soliton) and quasilinear radiation [17]. Here we will adopt a phenomenological description of the intensity distribution and the correlation properties of the output field based on the prescribed form of the solution as the sum of statistically independent soliton pulse shapes with prescribed statistical properties.

The single-soliton solution of (2) in soliton units is given by

$$u_s(\tau,\xi) = 2\eta\,\mathrm{sech}[4\eta v\tau + 2\eta(\xi-\xi_0)] \times \exp\{-i[2v\xi + 2\tau(v^2-\eta^2) - \phi]\}, \tag{4}$$

where the parameters η and v are related to the soliton's amplitude A and "velocity" (i.e., the angle of incidence θ), while the parameters ξ_0 and ϕ are the soliton's initial position and global phase. The total power of an individual soliton (or rather its transverse part in the x plane), $P = \int|E|^2dx$, is simply proportional to its amplitude: $P = 4\eta\tilde{I}L = 4\eta n_0/|n_2|\beta_0^2L$.

The justification for this approach is presented in the following Sec. IV where a more rigorous IST-based analysis is performed. It is these soliton constituents that contribute to the tails of the intensity distribution $P(I)$ as the linear radiation quickly disperses away from the aperture. Let us now assume the regime where the density of solitons is not too high so that the average minimal distance between the solitons is larger than the average width of a soliton—a regime that can be called an asymptotically free regime. Then each soliton contributes independently to the intensity distribution (the interference effects are neglected), and we may consider the contribution from each individual soliton separately. For the single-soliton solution of the NLSE (1) in real-world units the intensity at a certain point x is given by

$$I(x;\eta,v,x_0,\tau) = 4\eta^2\tilde{I}\,\mathrm{sech}^2\left[2\eta\left(\frac{x-x_0}{L} + 2v\tau\right)\right], \tag{5}$$

where 2η is the amplitude of the soliton in the dimensionless soliton units, $2v$ is its velocity, and x_0 is the intial position of the soliton center (in micrometers). As the input is random, the amplitude, velocity, and initial position of the soliton are also random variables. As for their joint probability density function $P(v,x_0,\eta)$, we shall make an assumption which is supported both by numerical simulations and by the following Zakharov-Shabat eigenvalue analysis (see below). Namely, we assume that the soliton velocity parameter v is independent of the other variables and its distribution is uniform over a symmetric interval $[-\Delta v/2,\Delta v/2]$. This immediately means that for a soliton emitted from the origin the position shift due to the fluctuating velocity is also a uniformly distributed random variable in the interval $[-\tilde{\Delta}/2,\tilde{\Delta}/2]$, where $\tilde{\Delta} = 2\Delta v\tau L$ and $\tau = Z/L_d$ is the propagation distance in soliton units.

The conditional probability density of having the value of intensity in the vicinity of I given the amplitude of the soliton, 2η, is then given by

$$P(I|\eta;x,\tau) = \left\langle \frac{1}{\Delta v}\int_{-\Delta v/2}^{\Delta v/2} \delta[I - I(x;\eta,v,x_0,\tau)]dv \right\rangle, \quad (6)$$

where $I(x;\eta,v,x_0,\tau)$ is given by Eq. (5) and the angular brackets denote additional averaging with respect to the marginal PDF of the initial positions $P(x_0|\eta)$.

In order to perform the averaging analytically we will consider only the high-intensity tails of the PDF when the typical soliton width, $L/2\eta$, is much smaller than the width of the position distribution, $\tilde{\Delta}$. Additionally we will assume that the propagation distance τ is large enough that $\tilde{\Delta} \gg L$, and therefore the fluctuations in the soliton initial position x_0 are negligible when compared to those due to the random velocity $2v$. After all these assumptions the result of integration of (6) can be presented as

$$P(I|\eta;x) = \frac{L}{\tilde{\Delta}} \frac{\sqrt{\tilde{I}}}{I\sqrt{4\eta^2\tilde{I} - I}}\theta[4\eta^2\tilde{I} - I], \quad |x| < \tilde{\Delta}/2, \quad (7)$$

where $\eta \gg L/2\tilde{\Delta}$ and $I \gg 16\eta^2\tilde{I}\exp[-8\eta\Delta v\tau]$.

If the number of produced solitons is $n > 1$ then it is relatively straightforward to derive the average minimal distance between neighboring solitons, which is given by $\tilde{\Delta}/(n^2+1)$. As we have assumed that the width of each soliton is much smaller than the average minimal intersoliton distance, this implies that the condition for the amplitude is in fact $\eta \gg L(n^2+1)/2\tilde{\Delta}$.

Finally, to get the marginal intensity distribution $P(I)$, we need to average Eq. (7) over all realizations of the soliton amplitude 2η. Assuming that the marginal PDF $P_\eta(\eta)$ is known and is the same for all realizations with different soliton numbers, the result reads

$$P(I) = \langle n\rangle \frac{1}{4\Delta v\tau}\frac{1}{I}\int_0^\infty P_\eta(\sqrt{I/4\tilde{I}}\,\cosh z)dz, \quad (8)$$

where $I \gg [\tilde{I}/(2\Delta v\tau)^2](\langle n\rangle^2+1)^2$, the factor $\langle n\rangle$ takes into account that for each realization all n solitons contribute equally and independently to the intensity, and we neglect the effects of interference and soliton collisions (i.e., overlap).

IV. IST-BASED ANALYSIS

Many properties of the evolving solution of the NLSE (2), including the number of emerging solitons, their amplitudes, energies, and velocities can be established by means of the so-called Zakharov-Shabat spectral problem (ZSSP) [17]:

$$i\frac{\partial\psi_1}{\partial\xi} + u\psi_2 = \zeta\psi_1, \quad -u^*\psi_1 - i\frac{\partial\psi_2}{\partial\xi} = \zeta\psi_2. \quad (9)$$

Here the complex initial field $u(0,\xi)$ plays the role of the "potential" while the complex eigenvalues ζ can have both discrete and continuous values. It is the discrete spectrum $\zeta_n = v_n + i\eta_n$ which determines the soliton part of the solution, and in the case of the single-soliton solution the parameters v and η are exactly the ones featured in Eq. (4).

We will start with numerical Monte Carlo simulations for the number of emerging solitons as well as their amplitudes and phases. In the Monte Carlo simulations we took 4000 runs with the parameters of the random Zakharov-Shabat potential given in Table I. Those were chosen to be close to the experimental values of Ref. [9]. We used a well-documented method for finding the discrete eigenvalues of (9) which relies on the fact that these are the complex roots of the associated first Jost coefficient $a(\zeta)$ and can be found by recursive subdivision of the complex space into rectangles and application of the argument principle to each small rectangle (see Refs. [18] for further details). We performed two runs with different values of the initial average power $P = a^2NdL$. The first one corresponds to peak power of $P = 1$ kW and the second to $P = 5$ kW, and we will refer to these as "low-power" and "high-power" runs, respectively (keeping in mind that these labels correspond to the power of the initial disordered field). Other runs with different values of the input parameters (like the initial power and the correlation length) were also performed, but their results were qualitatively the same as in the high-power or low-power runs so to keep the presentation simple and illustrative we report only the results for these two. Because the input is random the number of emerging solitons will fluctuate around the mean. In Fig. 1 we present a distribution of the number of emerging solitons for the values

TABLE I. The main parameters of the simulations for the focusing case.

Parameter	Value
Size of the aperture L (μm)	50
Thickness of the slab d (μm)	1.5
Size of the computational domain L' (μm)	4096
Total number of points M'	8192
Number of points resolving the aperture M	100
Total number of random modes N	2048
Maximum propagation distance z (μm)	8000
Linear refractive index n_0	3.3
Propagation constant β_0 (μm^{-1})	12.61
Nonlinear coefficient n_2 (cm^2/GW)	1.67×10^{-4}
Initial correlation length S_0 (μm)	2
Diffraction length L_d (mm)	33.9
Normalization intensity $\tilde{I}$ (GW/cm^2)	0.05
Window used for collecting histograms Δ (μm)	1024

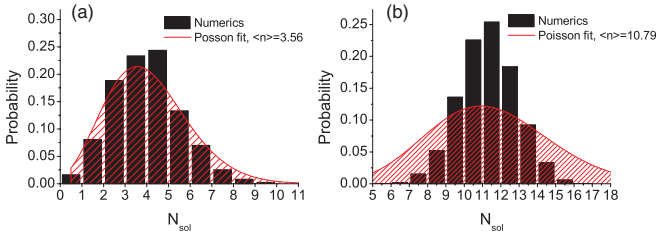

FIG. 1. (Color online) The distribution of the number of emerging solitons for low-intensity (a) and high-intensity (b) regimes.

of parameters given in Table I, together with the corresponding Poisson fits.

One can clearly see that the number of solitons does approximately follow the Poisson distribution for low intensity (small number of solitons) but this approximation breaks down for the high-power run when the number of solitons is higher. Similar results were reported earlier in Ref. [16] in the context of nonlinear fiber optics.

Next, shown in Fig. 2 (as dashed and dotted lines) are the numerical marginal PDFs for the real and imaginary parts of the ZS eigenvalues $P_v(v)$ and $P_\eta(\eta)$ which are just the scaled distributions for the soliton final position and amplitude. A

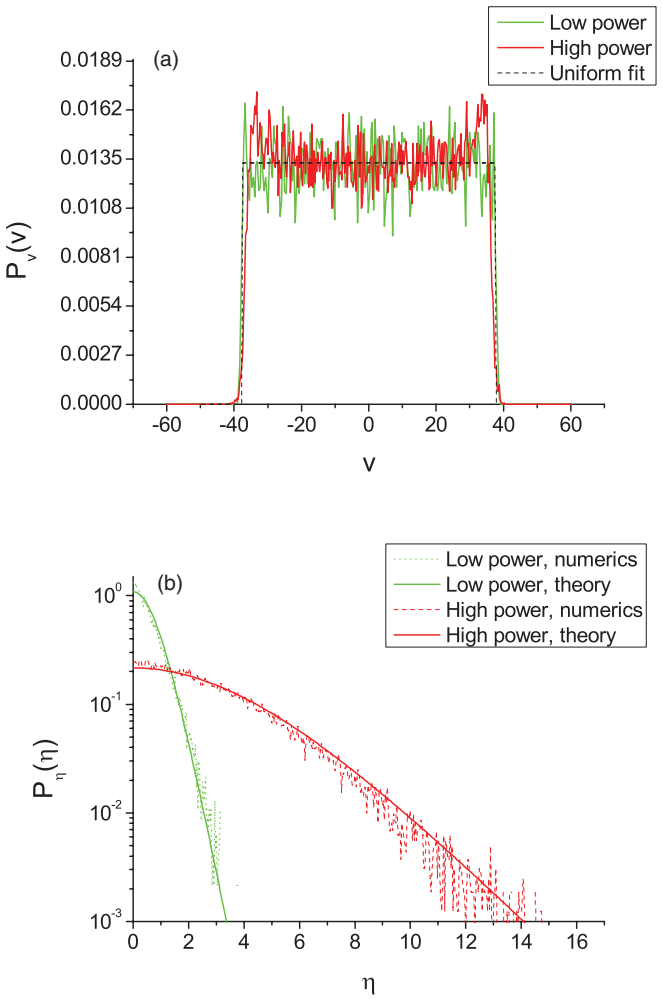

FIG. 2. (Color online) The marginal PDFs of the real (a) and imaginary (b) parts of the ZSSP eigenvalues.

separate Monte Carlo run (not shown) has demonstrated that the numerical joint distribution $P(v,\eta)$ is indeed separable so the marginal distributions are sufficient. One can see that the PDF for the real part $P_v(v)$ is close to uniform with the width $\Delta v = 75.8$, which supports the assumptions made earlier in Sec. III. Indeed, assuming that solitons are created in the area localized by the relative small aperture size L, it follows that the uniform distribution of the real parts of the eigenvalues with support Δv yields a uniform distribution of soliton positions at the output facet with the support $\tilde{\Delta} = 2\Delta_v(L/L_d)z = 1788\ \mu$m for the values of parameters given in Table I. Moreover our numerical data also show that the support of the distribution Δ does not depend on the average power P, but rather solely on the input correlation length S_0, where, as expected, shorter input correlation distances yield broader distributions for v.

In the limit of a δ-correlated initial field the results above can be confirmed analytically. Indeed, one can formally define a 2D density of states (eigenvalues) of the non-Hermitian ZSSP (9) as

$$\rho(v,\eta) = \frac{1}{L}\sum_n \langle \delta(v - v_n)\delta(\eta - \eta_n)\rangle, \tag{10}$$

where the summation is performed over all discrete eigenvalues for each realization and the averaging is performed over all possible realizations. It is clear that the density of states $\rho(v,\eta)$ is (up to a normalization factor) the probability density of having a level in the vicinity of point (v,η). Therefore if one knows the density of states it is possible in principle to determine the desired level distribution. In Ref. [19] this quantity was obtained analytically in the limit of the Stratonovich δ-correlated potential when the support of the potential L is large. The result reads

$$\rho(v,\eta) = \frac{1}{\pi D}\frac{(\eta/D)\coth(\eta/D) - 1}{\sinh^2(\eta/D)}, \quad D \equiv \frac{S_0}{L}\frac{I_0}{2\tilde{I}}. \tag{11}$$

One can show [20] that in the strict mathematical limit of Stratonovich white noise the result above is inapplicable, but it holds for any physical process with a symmetric field correlation function of finite but small radius, like, e.g., (3), when S_0 is much less than the aperture length. One immediately notices that the quantity $\rho(v,\eta)$ does not depend on the real part of the eigenvalue, v. Therefore the total number of states with a given imaginary part η is infinite, i.e., the probability density function $P(v,\eta)$ is not normalizable in the v direction. This is again the consequence of the idealized nature of the white noise, and for systems with finite correlation radius all the quantities in question are of course finite. This is indeed confirmed by the numerical results discussed above—as we can see, the marginal PDF $P_v(v)$ is almost flat, it does not depend on the value of the initial power, and its support diverges in the white-noise limit. Thus the analytical result Eq. (11) in the short-correlated limit explains both the separability of the eigenvalue distribution and the flat marginal distribution $P(v)$ observed numerically. One can now immediately derive the analytical expression for the normalized marginal probability $P_\eta(\eta)$:

$$P_\eta(\eta) = \frac{2}{D}\frac{(\eta/D)\coth(\eta/D) - 1}{\sinh^2(\eta/D)}. \tag{12}$$

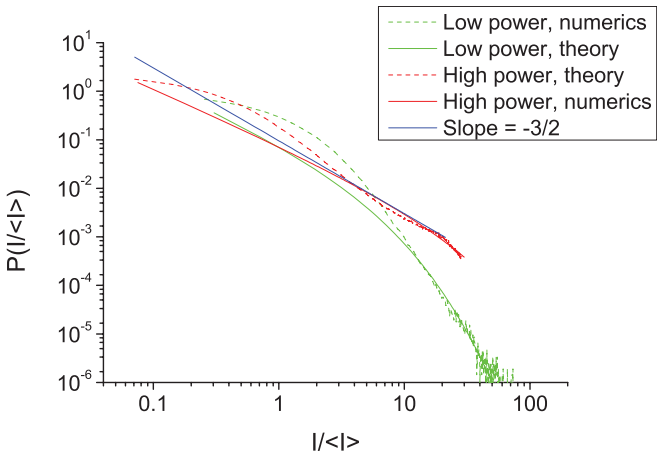

FIG. 3. (Color online) The PDF of the field intensity obtained from the direct numerical simulations of Eq. (2) and the one reconstructed from the IST theory via formula (13). The average intensity was $\langle I\rangle = 3.28 \times 10^{-2}$ GW/cm^2 (low power) and $\langle I\rangle = 13.3 \times 10^{-2}$ GW/cm^2 (high power).

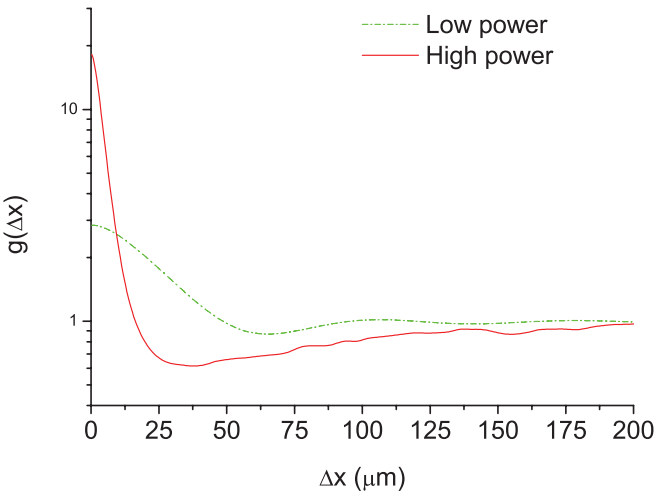

FIG. 4. (Color online) The intensity correlation function obtained from the direct numerical simulations of Eq. (2).

For the specific parameters of our numerical simulations the last formula in Eq. (11) yields $D = 0.61$ for the low-power run and $D = 3.08$ for the high-power run. The corresponding analytical curves (12) are plotted as solid lines in Fig. 2(b) and one can observe a rather good agreement with the numerics.

Plugging the amplitude PDF (12) into the expression (8), one obtains

$$P_{\rm est}(I) = \langle n\rangle \frac{L}{2\tilde{\Delta} D}\frac{1}{I} f\left(\sqrt{\frac{I}{4\tilde{I}D^2}}\right),$$
$$f(x) = 2\int_0^\infty \frac{x\cosh z\coth(x\cosh z) - 1}{\sinh^2(x\cosh z)}dx. \tag{13}$$

For large values of the argument $x \gg 1$ we have $f(x) \approx 8xK_1(2x)$ and we obtain the asymptote $P(I) \propto I^{-3/4}\exp[-(I/D^2\tilde{I})^{1/2}]$ as the high-intensity tail of the distribution. It turns out that Eq. (13) provides a remarkably good approximation of the tails of the intensity PDFs—see Fig. 3, where we compare it with the results of the direct Monte Carlo simulations of the NLSE propagation (again 4000 realizations were used). One can see that our analytical result works rather well for $I > 10\langle I\rangle = 0.328$ GW/cm^2 (low-power limit) and 1.33 GW/cm^2 (high-power limit). The discrepancies at low intensities are due to the fact that (i) at low intensity the contribution of the radiation (completely ignored in our semianalytical scheme) becomes non-negligible and (ii) the dilute-soliton-gas approximation is not valid for very low-power (and hence very wide) solitons that overlap and interfere significantly, which violates the assumptions used in deriving Eq. (13). For the overlapping solitons the phase interference becomes an important effect diminishing the soliton contribution to the intensity, which explains why the analytical result overestimates the probability of low-intensity events. One can also observe that the numerical PDFs for both high- and lower-power values have an interesting structure with an inflection point. This inflection point corresponds to the crossover between the regime of well-separated high-intensity pulses and that of broad, interfering low-intensity solitons. Finally we plot a $-3/2$ slope line as a reference. In Ref. [9] it was suggested that this slope is close to universal, which would imply some universal power-law tails. Our results show that this is not so. While it does work well as the best fit in the region around the inflection point in the high-power case, it is well off the mark in the low-power case. Also, for the high-power case one can clearly see a crossover to the exponential tail as predicted by Eq. (13). So we must conclude that there is no evidence of a universal (i.e., independent of the initial power) power-law asymptote which describes the whole tail of the intensity distribution, as clearly seen from Fig. 3.

Following Ref. [9], we can also introduce a normalized intensity autocorrelation function as

$$g(\Delta x) = \frac{\int\langle I(x)I(x+\Delta x)\rangle dx}{\int\langle I(x)\rangle\langle I(x+\Delta x)\rangle dx}, \tag{14}$$

where $I(x) = |E(x)|^2$ is the fluctuating intensity of the beam. For a linear medium it can be shown that $g(0) = 2$ and then it falls to $g(\infty) = 1$ over a characteristic length scale—the intensity correlation length S (also called the "speckle size"). In Fig. 4 we plot the correlation function $g(\Delta x)$ obtained from the same numerical run as the other statistics. If we compare the limiting values of the intensity correlation function with the results of the Appendix, which were obtained using only the soliton component of the solution, we can see that the limiting value $g(\infty)$ is very close to unity while theory gives the value $\langle n^2\rangle/\langle n\rangle^2 - 1/\langle n\rangle \approx 0.92$ (for both high- and low-power runs), which is close. As for the opposite limit, one can see from Fig. 4 that the limiting values $g(0) = \langle I^2\rangle/\langle I\rangle^2 \approx 2.85$ (low power) and $\approx$18.5 (high power) are far smaller than the predictions of Eq. (A6) [where the moments of η were taken from the distribution (12)], $g(0) \approx 17$ (low power) and $g(0) \approx 26.5$ (high power). This discrepancy can be easily explained when one looks at Fig. 3, where it is clear that the first two moments of the intensity determining $g(0)$ are formed by the region $I \sim \langle I\rangle$, where the nonsoliton part of the radiation is important and also soliton pulses are wide enough to cover most of the sampling region. However,

the analytical prediction of the Appendix for the correlation length itself, $S = L/2\sigma_\eta = L/2D \approx 40$ μm (low power) and ≈ 8 μm (high power) holds remarkably well. If we recall the definition of the parameter D we get (in the short-correlated limit) a simple relation between the observed correlation length S, the initial correlation length S_0, and the average initial intensity I_0:

$$S = \frac{L^2 \tilde{I}}{S_0 I_0}. \tag{15}$$

So the observed correlation length is inversely proportional to the initial correlation length and the initial average intensity (or power). The latter fact confirms the experimental results of Ref. [9]. Also, the correlation length in this regime does not depend on the propagation distance τ (i.e., is saturated), which together with the scaling law $g(0) \propto \tau$ [see Eq. (A6)] coincide with the results obtained in [9] by qualitative considerations.

V. DEFOCUSING CASE

Let us now turn attention to the defocusing case where $n_2 < 0$. The experimental results of [9] show qualitatively different behavior of both the correlation function and the intensity PDF. In particular, the correlation strength $g(0)$ goes down with the intensity of the initial speckle field (unlike in the focusing case) and the intensity distributions also look markedly different. Here we will again employ the inverse scattering method to study the resulting intensity PDFs. A similar problem for the defocusing case was studied previously in [21] using the asymptotic far-field expansion developed by Manakov [17,22]. The ZSSP for the focusing and defocusing cases differ only by the sign of the potential in the second equation, so that in the defocusing case one will have

$$i\frac{\partial \varphi_1}{\partial \xi} + u\varphi_2 = \zeta \varphi_1, \quad u^*\varphi_1 - i\frac{\partial \varphi_2}{\partial \xi} = \zeta \varphi_2. \tag{16}$$

If we assume zero boundary conditions at infinity for the defocusing NLSE, no bright (or dark) solitons are formed and the far field is formed solely by dispersive waves.

It is known that asymptotically at large z the field intensity $I(x,z)$ in real-world units is given by the following formula [17,21,22]:

$$I(x,z) = \frac{\tilde{I} L_D}{2\pi z} \ln \left| a\left(-\frac{L_D}{2L}\frac{x}{z}\right)\right|^2, \tag{17}$$

where $a(\zeta)$ is determined via the particular solution of (16) subject to the following boundary conditions [17]:

$$\phi(0;\zeta) = \begin{pmatrix} 1 \\ 0 \end{pmatrix}, \quad \phi(1;\zeta) = \begin{pmatrix} a(\zeta)e^{-i\zeta} \\ b(\zeta)e^{i\zeta} \end{pmatrix}. \tag{18}$$

Here the spectral parameter ζ is real and we have assumed for definiteness that the initial support of the pulse is $[0,L]$ in real-world units. The coefficients $a(\zeta)$ and $b(\zeta)$ are called the first and second Jost coefficients, respectively, and satisfy the condition $|a|^2 - |b|^2 = 1$. Using the invariant imbedding approach already developed for the focusing case (see, e.g., [23]) we can introduce the functions $a(\zeta;\xi) = \varphi_1(\xi)e^{i\zeta\xi}$, $b(\zeta;\xi) = \varphi_2(\xi)e^{-i\zeta\xi}$, for which we will have the following system of equations:

$$\begin{aligned} \frac{\partial a(\zeta,\xi)}{\partial \xi} &= ib(\zeta,\xi)e^{2i\zeta\xi}u(\xi), \quad a(\zeta;0) = 1, \\ \frac{\partial b(\zeta,\xi)}{\partial \xi} &= -ia(\zeta,\xi)e^{-2i\zeta\xi}u^*(\xi), \quad b(\zeta;0) = 0. \end{aligned} \tag{19}$$

The Jost coefficients are recovered as $a(\zeta) = a(\zeta,1)$ and $b(\zeta) = b(\zeta,1)$. Note that, as $u(\xi)$ may be considered Gaussian with the correlation function given by (3) (in real-world units), the phase factor $\exp(2i\zeta\xi)$ can be absorbed into the definition of the random field $u(\xi)$ so that the statistics of both Jost coefficients become independent of the spectral parameter ζ. From (17) it immediately follows that asymptotically the values of the field intensity become uncorrelated, i.e., the correlation function $g(\Delta x)$ tends to unity across the transverse dimension of the beam as long as the distance z is large. Let us parametrize $|a|$ and $|b|$ as $\cosh\chi$ and $\sinh\chi$, respectively, and introduce a phase difference between the two Jost coefficients: $\varphi = \mathrm{Arg}[a] - \mathrm{Arg}[b]$. Then for these two real quantities one obtains the system of equations

$$\begin{aligned} \frac{d\chi}{d\xi} &= -\mathrm{Im}[e^{-i\varphi}u(\xi)], \quad \chi(0) = 0, \\ \frac{d\varphi}{d\xi} &= 2\coth 2\chi \,\mathrm{Re}[e^{-i\varphi}u(\xi)], \end{aligned} \tag{20}$$

where the value of the initial phase $\varphi(0)$ is chosen so that the derivative $\varphi'(0)$ is finite (see, e.g., [23]). In the δ-correlated limit we obtain from the system (20) (treated in the Stratonovich sense) the following Fokker-Planck equation for the joint PDF $P(\chi,\varphi;\xi)$ [24]:

$$\frac{\partial P}{\partial \xi} = -D\frac{\partial}{\partial \chi}[\coth(2\chi)P] + \frac{D}{2}\frac{\partial^2 P}{\partial \chi^2} + 2D\coth^2(2\chi)\frac{\partial^2 P}{\partial \varphi^2}. \tag{21}$$

According to (17) and (18), the statistics of the intensity is determined by the statistics of the quantity $\ln\cosh\chi$ at $\xi = 1$ so we can integrate out the dependence on the angular variable φ using the periodic boundary conditions and make the substitution $P(\chi;\xi) = Y(\chi;\xi)\sinh 2\chi$ for the resulting marginal distribution of the random variable χ. The resulting equation reads

$$\begin{aligned} \frac{\partial Y}{\partial \xi} &= \frac{(D/2)}{\sinh 2\chi}\frac{\partial}{\partial \chi}\left[\sinh(2\chi)\frac{\partial Y}{\partial \chi}\right], \\ Y(\chi;0) &= \delta(\chi)/\sinh(2\chi). \end{aligned} \tag{22}$$

This equation is known in the theory of stochastic processes [2,25] and it has the solution in quadratures

$$Y(\chi;1) = \sqrt{\frac{1}{\pi D^3}}e^{-D/2}\int_\chi^\infty \frac{\chi' \exp(-\chi'^2/2D)}{\sqrt{\cosh(2\chi') - \cosh(2\chi)}}d\chi'. \tag{23}$$

Finally, for the intensity PDF one has the following expression:

$$\begin{aligned} P(I) = \frac{2\pi z}{\tilde{I}L_D}\exp\left[\frac{2\pi z}{L_D}\frac{I}{\tilde{I}}\right] Y\left\{\frac{\pi z}{L_D}\frac{I}{\tilde{I}}\right. \\ \left. + \ln\left[1 + \sqrt{1 - \exp\left(-2\frac{\pi z}{L_D}\frac{I}{\tilde{I}}\right)}\right]; 1\right\}. \end{aligned} \tag{24}$$

TABLE II. The main parameters of the simulations for the defocusing case.

Parameter	Value
Size of the aperture L (μm)	50
Thickness of the slab d (cm)	2
Size of the computational domain L' (mm)	8.192
Total number of points M'	16384
Number of points resolving the aperture M	100
Total number of random modes N	4096
Linear refractive index n_0	1.3
Propagation constant β_0 (μm^{-1})	15.62
Nonlinear coefficient n_2 (cm^2/W)	-2.6×10^{-8}
Initial correlation length S_0 (μm)	2
Diffraction length L_d (mm)	39.04
Normalization intensity $\tilde{I}$ (W/cm^2)	82.00
Window used for collecting histograms Δ (μm)	512

An interesting feature of the distribution above is that it is self-similar in the propagation distance z, i.e., the PDF of the quantity $y \equiv zI/\tilde{I}L_D$ is universal and depends only on the disorder level D. The tail of this PDF is Gaussian,

$$P(y) = \frac{\sqrt{y}}{D}\, e^{-D/2}\, e^{-y-y^2/2D}, \quad y \gg 1. \tag{25}$$

Also, as mentioned before, in this far-field limit the field values at the different points are uncorrelated so that $g(\Delta x) \equiv 1$, for $\Delta x \geqslant S_0$.

To test the analytical result above, we again choose the model parameters close to those considered in experiments [9]. Namely, we choose ethanol with an absorbing dye as a defocusing nonlinear medium at the wavelength of 552 nm and assume the values of parameters given in Table II.

Although in the real experiments the pulse attenuation was quite high at the length scale considered, we can still use these parameters for illustrative purposes. In our simulations we assumed a fixed averaged value of the input power, $P = 6$ W, which correspond to the effective nonlinear length $L_{NL} = (|n_2|\beta_0 I_0/n_0)^{-1} = 5.33$ mm. The simulations were performed for three values of the propagation distance z comparable to the nonlinear length. The results are given in Fig. 5.

One can clearly see that, depending on the propagation distance z, there are two regimes with two types of statistics. When the propagation distance is smaller than the nonlinear length L_{NL}, the nonlinear term in Eq. (2) can be neglected, i.e., the propagation is linear and as mentioned before the intensity PDF is exponential. It easy to check that in terms of the self-similar variable y the linear PDF is

$$P_{\rm lin}(y) = \frac{1}{2D}\, e^{-y/2D}.$$

When the distance exceeds the nonlinear length the far-field asymptotes (24) and (25) hold, and the shape of the PDF $P(y)$ becomes universal (with Gaussian tails). The intermediate values of the propagation distance fill the gap between the two limiting distributions (as clearly seen in Fig. 5).

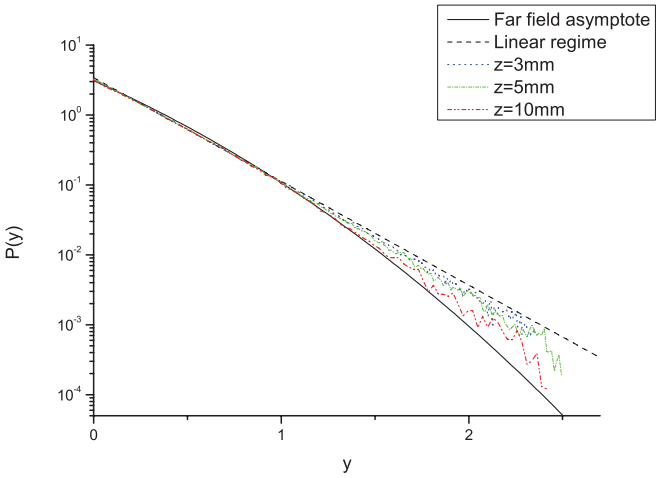

FIG. 5. (Color online) The PDF of the self-similar variable y for different values of the propagation distance.

VI. CONCLUSION

To conclude, we have studied both analytically and numerically the statistics of the intensity distribution of a disordered short-correlated pulse propagating in a nonlinear medium under conditions close to those experimentally observed in Ref. [9]. In the limit of the δ-correlated pulse, when the initial correlation length (speckle size) is much smaller than the aperture size, we provide analytical expressions for the intensity distribution for both focusing and defocusing media. It turns out that the power-law tails reported in [9] are not universal and represent an approximate fit to a transitional area followed by an exponential asymptote in the focusing case and a Gaussian asymptote in the defocusing case. For the latter a universal analytical formula for the intensity PDF is given in the regime when the propagation length (the length of the beam) is larger than the nonlinear length. Also, in the focusing case, a simple expression is given for the intensity correlation width S [formula (15)] which relates it to the initial correlation width (speckle size) S_0 and the average intensity of the source I_0, confirming the results of Ref. [9]. This formula supplements the relation $g(0)S = 2\lambda z/L$ obtained in Ref. [9] using quantitative arguments and thus allows one to estimate not only the linear size of the object L, but also its average intensity I_0 and the correlation radius S_0 (or rather the product of the two) when the system is in the soliton regime (high power, high number of speckle beamlets).

ACKNOWLEDGMENTS

We would like to thank Yaron Silberberg for drawing our attention to the problem and Ehud Altman for stimulating discussions. S.D. would like to thank the Department of Physics of Complex Systems at Weizmann Institute of Science for its warm hospitality.

APPENDIX: THE DERIVATION OF THE SOLITON INTENSITY CORRELATION FUNCTION

For a single soliton with the intensity profile (5) and a uniform position distribution, it is possible to calculate the

intensity correlation function g_1 provided that the typical soliton amplitude σ_η is much greater than the ratio $1/(4\Delta v\tau)$, i.e., all typical soliton pulse realizations (as well as the correlation function itself) have widths much smaller than the size of the region where solitons are eventually distributed, $\tilde{\Delta}$. Then one obtains

$$\langle I_1(x)\rangle = \langle I_1(x+\Delta x)\rangle = \frac{2\tilde{I}}{\Delta v\tau}\langle\eta\rangle \equiv I_1$$

and

$$\langle I_1(x)I_1(x+\Delta x)\rangle = \frac{16\tilde{I}^2}{\Delta v\tau}\left\langle\frac{\eta^3}{\sinh^2 q}(q\coth q-1)\right\rangle,$$

where $|x|,|x_0|,\Delta x \ll \tilde{\Delta}$ and $q = 2\eta\Delta x/L$. So for the one-soliton correlation function we obtain

$$g_1(\Delta x) = 4\Delta v\tau\left\langle\frac{\eta^3}{\sinh^2 q}(q\coth q-1)\right\rangle\Big/\langle\eta\rangle^2, \quad \text{(A1)}$$

where the averaging in the RHS is performed over the amplitude distribution. The relative strength of intensity fluctuations for one soliton is given by

$$g_1(0) = \frac{4\Delta v\tau}{3}\frac{\langle\eta^3\rangle}{\langle\eta\rangle^2}. \quad \text{(A2)}$$

Next, let us consider a train of n solitons with statistically independent parameters and random, uniform phases. First we consider realizations where exactly n solitons are created. Then we have

$$\langle I(x)\rangle = n\langle I_1(x)\rangle = nI_1$$

and

$$\begin{aligned}\langle I(x)I(x+\Delta x)\rangle &= n(n-1)\langle I_1(x)\rangle\langle I_1(x+\Delta x)\rangle + n\langle I_1(x)I_1(x+\Delta x)\rangle \\ &\quad + n(n-1)|\langle E_1(x)E_1^*(x+\Delta x)\rangle|^2,\end{aligned}$$

where $E_1(x)$ is the single-soliton field (4) in real-world units. Performing additional averaging over all realizations with different numbers of solitons as well as over the spatial coordinate x (denoted by an overbar), we arrive at

$$g(\Delta x) = \frac{1}{\langle n\rangle}g_1(\Delta x) + \left(\frac{\langle n^2\rangle}{\langle n\rangle^2} - \frac{1}{\langle n\rangle}\right) \times\left(1 + \frac{\overline{|\langle E_1(x)E_1^*(x+\Delta x)\rangle|^2}}{I_1^2}\right). \quad \text{(A3)}$$

Again, if we assume that the typical width of a soliton is much smaller than its positional support $\tilde{\Delta}$, one can show that the field correlation term is position independent and is given by

$$\begin{aligned}&\frac{1}{I_1^2}|\langle E_1(x)E_1^*(x+\Delta x)\rangle|^2 \\ &= \left|\left\langle\frac{\eta}{2\langle\eta\rangle}\int_{-\infty}^{\infty}\mathrm{sech}[y]\mathrm{sech}[y+q]e^{-i(q/4\tau\eta^2)y}dy\right\rangle\right|^2 \quad \text{(A4)}\end{aligned}$$

If additionally $\Delta x \ll \min[4\tau\langle\eta\rangle, L\tau^{1/2}]$ (i.e., the random phase shift $\Delta\phi = 2v\Delta x/L$ can be neglected) the above simplifies to

$$\frac{1}{I_1^2}|\langle E_1(x)E_1^*(x+\Delta x)\rangle|^2 = \left\langle\frac{\eta q}{\langle\eta\rangle\sinh q}\right\rangle^2. \quad \text{(A5)}$$

The strength of fluctuations is given by

$$g(0) = \frac{\langle I^2\rangle}{\langle I\rangle^2} = \frac{4\Delta v\tau}{3\langle n\rangle}\frac{\langle\eta^3\rangle}{\langle\eta\rangle^2} + 2\left(\frac{\langle n^2\rangle}{\langle n\rangle^2} - \frac{1}{\langle n\rangle}\right). \quad \text{(A6)}$$

When the argument of the correlation function is large, i.e., the inequality $L/2\Delta x \ll \sigma_\eta$ holds, the function being averaged in Eq. (A1) decays much faster than the PDF P_η, which can be used to obtain the following asymptote:

$$g_1(\Delta x) \approx \frac{3\zeta(3)}{8}\frac{\Delta v\tau P_\eta(0)}{\langle\eta\rangle^2}\left(\frac{L}{\Delta x}\right)^4, \quad \text{(A7)}$$

where $\Delta x \gg L/2\sigma_\eta$ is assumed. For the full correlation function, if one assumes additionally that $\Delta x \gg L\max[1/2\sigma_\eta, \sqrt{\tau}]$, the field correlation contribution (A4) contains the prefactor $(L/\Delta x)^4$ multiplied by a highly oscillating integral, so its contribution is neglected and one can write down

$$g(\Delta x) \approx g(\infty) + \frac{g_1(\Delta x)}{\langle n\rangle} \quad \text{(A8)}$$

with $g_1(\Delta x)$ given by Eq. (A7) above.

One can see that the correlation function reaches its asymptotic value $g(\infty) = \langle n^2\rangle/\langle n\rangle^2 - 1/\langle n\rangle$ following a power law. If the number of emerging solitons follows a Poisson distribution (where the variance is equal to the mean) the limiting value of the correlation function is $g(\infty) = 1$, as in the linear case. For the correlation radius S one gets the estimate $S \approx L/2\sigma_\eta$. The latter formula has a transparent physical meaning: the correlation length S is a typical speckle size in any optical system. In the regime considered here, bright solitons play the role of "nonlinear speckles" so the typical speckle size is the width of a typical soliton, which is given by $L/2\sigma_\eta$.

[1] B. I. Shraiman and E. D. Siggia, Phys. Rev. E **49**, 2912 (1994); G. Falkovich, I. Kolokolov, V. Lebedev, and A. Migdal, *ibid.* **54**, 4896 (1996).

[2] I. M. Lifshitz, S. A. Gredeskul, and L. A. Pastur, *Introduction to the Theory of Disordered Systems* (Wiley, New York, 1988).

[3] G. Samelsohn, S. A. Gredeskul, and R. Mazar, Phys. Rev. E **60**, 6081 (1999).

[4] D. R. Solli *et al.*, Nature (London) **450**, 1054 (2007); B. Kibler *et al.*, Phys. Lett. A **375**, 3149 (2011); J. M. Soto-Crespo, Ph. Grelu, and N. Akhmediev, Phys. Rev. E **84**, 016604 (2011).

[5] K. Hammani, A. Picozzi, and C. Finot, Opt. Commun. **284**, 2594 (2011).

[6] J. M. Dudley, G. Genty, and B. J. Eggleton, Opt. Express **16**, 3644 (2008).

[7] S. Vergeles and S. K. Turitsyn, Phys. Rev. A **83**, 061801(R) (2011); **84**, 067802 (2011).
[8] E. Iannone, F. Matera, A. Mecozzi, and M. Settembre, *Nonlinear Optical Communication Networks* (John Wiley & Sons, New York, 1998).
[9] Y. Bromberg, Y. Lahini, E. Small, and Y. Silberberg, Nat. Photonics **4**, 721 (2010).
[10] R. Hanbury Brown and R. Q. Twiss, Nature (London) **178**, 1046 (1956); **177**, 27 (1957).
[11] J. W. Goodman, *Speckle Phenomena in Optics* (Roberts & Company, Greenwood Village, CO, 2007).
[12] M. Schellekens *et al*., Science **310**, 648 (2005); S. Fölling *et al*., Nature (London) **434**, 481 (2005).
[13] N. Shnerb and M. Kaveh, Phys. Rev. B **43**, 1279 (1991).
[14] Y. S. Kivshar and G. P. Agrawal, *Optical Solitons* (Academic Press, San Diego, 2003).
[15] M. Mitchell and M. Segev, Nature (London) **387**, 880 (1997); C. Rotschild *et al*., Nat. Photonics **2**, 371 (2006); A. Picozzi, Opt. Express **16**, 7818 (2008).
[16] S. K. Turitsyn and S. A. Derevyanko, Phys. Rev. A **78**, 063819 (2008).
[17] S. Manakov, S. Novikov, L. Pitaevskii, and V. Zakharov, *Theory of Solitons* (Consultants Bureau, New York, 1984); V. E. Zakharov and A. B. Shabat, Zh. Exp. Teor. Fiz. **61**, 118 (1971) [Sov. Phys. JETP **34**, 62 (1972)].
[18] S. Burtsev, R. Camassa, and I. Timofeyev, J. Comput. Phys. **147**, 166 (1998); G. Boffetta and A. R. Osborne, *ibid*. **102**, 252 (1992).
[19] P. Kazakopoulos and A. L. Moustakas, Phys. Rev. E **78**, 016603 (2008).
[20] S. A. Derevyanko, Phys. Rev. E **84**, 016601 (2011).
[21] F. G. Bass, Y. S. Kivshar, and V. V. Konotop, Zh. Eksp. Teor. Fiz. **92**, 432 (1987) [Sov. Phys. JETP **65**, 245 (1987)].
[22] S. V. Manakov, Zh. Eksp. Teor. Fiz. **65**, 1392 (1973) [Sov. Phys. JETP **38**, 693 (1974)].
[23] S. A. Derevyanko and J. E. Prilepsky, Phys. Rev. E **78**, 046610 (2008).
[24] H. Risken, *The Fokker-Planck Equation* (Springer, Berlin, 1984).
[25] S. Derevyanko, Opt. Lett. **33**, 2404 (2008).